# Kondo effects in carbon nanotubes: From SU(4) to SU(2) symmetry

Jong Soo Lim
*Department of Physics, Seoul National University, Seoul 151-742, Korea*
*and Department of Physics, Korea University, Seoul 136-701, Korea*

Mahn-Soo Choi*
*Department of Physics, Korea University, Seoul 136-701, Korea*
*and Department de Física, Universitat de les Illes Balears, E-07122 Palma de Mallorca, Spain*

M. Y. Choi
*Department of Physics, Seoul National University, Seoul 151-742, Korea*
*and Korea Institute for Advanced Study, Seoul 130-722, Korea*

Rosa López
*Department de Física, Universitat de les Illes Balears, E-07122 Palma de Mallorca, Spain*

Ramón Aguado
*Teoría de la Materia Condensada, Instituto de Ciencia de Materiales de Madrid (CSIC) Cantoblanco, 28049 Madrid, Spain*
(Received 4 August 2006; published 27 November 2006)

We study the Kondo effect in a single-electron transistor device realized in a single-wall carbon nanotube (NT). The $K$-$K'$ double orbital degeneracy of a NT, which originates from the peculiar two-dimensional band structure of graphene, plays the role of a pseudospin. Screening of this pseudospin, together with the real spin, can result in an SU(4) Kondo effect at low temperatures. In order to have such an exotic Kondo effect it is crucial that this orbital quantum number be conserved during tunneling. Experimentally, this conservation is not obvious and some mixing in the orbital channel may occur. Here we investigate in detail the role of mixing and asymmetry in the tunneling coupling and analyze how different Kondo effects, from an SU(4) symmetry to a two-level SU(2) Kondo effect, emerge depending on the mixing and/or asymmetry. We use four different theoretical approaches to address both the linear and nonlinear conductance for different values of external magnetic field. Our results point out clearly the experimental conditions to observe exclusively SU(4) Kondo physics. Although we focus on NT quantum dots (QDs) our results also apply to vertical quantum dots. We also mention that a finite amount of orbital mixing corresponds, in pseudospin language, to having noncollinear leads with respect to the orbital "magnetization" axis which defines the two pseudospin orientations in the carbon nanotube QD. In this sense, some of our results are also relevant to the problem of a Kondo QD coupled to noncollinear ferromagnetic leads.

DOI: 10.1103/PhysRevB.74.205119 PACS number(s): 75.20.Hr, 73.63.Fg, 72.15.Qm

## I. INTRODUCTION

The first observations of Kondo effect in semiconductor quantum dots (QDs)[1–3] spurred a great deal of experimental and theoretical activity over the last few years. Since these experimental breakthroughs, remarkable achievements have been reported, including the observation of the unitary limit,[4] the singlet-triplet Kondo effect,[5] Kondo effect in molecular conductors,[6] and the Kondo effect in QDs connected to ferromagnetic[7] and superconducting reservoirs,[8] just to mention a few.

Recently, Jarillo-Herrero *et al.* reported perhaps the most sophisticated example, namely, the observation of an orbital Kondo effect in a carbon nanotube (CNT) quantum dot (QD).[9] In these experiments it was shown that the delocalized electrons of the reservoirs can screen both the orbital pseudospin degree of freedom in the CNT QD (the $K$-$K'$ double orbital degeneracy of the two-dimensional band structure of graphene,) and the usual spin degree of freedom resulting in an SU(4) Kondo effect at low temperatures. In a recent paper,[10] we showed that quantum fluctuations between the orbital and spin degrees of freedom may indeed dominate transport at low temperatures and lead to this highly symmetric SU(4) Kondo effect. More recently, Sakano and Kawakami[11] have studied using the Bethe ansatz method at zero temperature and the noncrossing approximation (NCA) at finite temperatures the more general case where the quantum numbers of $N$ degenerate orbital levels are conserved, and found new interesting features of SU($2N$)-symmetric Kondo effect. Importantly, an SU(4) Kondo effect is possible provided that both the orbital and spin indexes are conserved during tunneling. This poses an interesting question about the nature of the nanotube-lead contact because, in principle, there is no special reason why the orbital degree of freedom in the CNT should be conserved during tunneling.

As we mentioned, this orbital pseudospin originates from the peculiar electronic structure of the nanotube.[9,12,13] The electronic states of a NT form one-dimensional electron and hole subbands as a result of the quantization of the electron wavenumber perpendicular to the nanotube axis $k_\perp$, which arises when graphene is wrapped into a cylinder to create a NT. By symmetry, for a given subband at $k_\perp = k_0$ there is a second degenerate subband at $k_\perp = -k_0$. Semiclassically, this orbital degeneracy corresponds to the clockwise (↻) or coun-

 

terclockwise ($\circlearrowleft$) symmetry of the wrapping modes. A plausible explanation of why this degree of freedom is preserved during tunneling could be that the QD is likely coupled to NT electrodes (the metal electrodes are deposited on top of the NT so maybe the electrons tunneling out of the QD enter the NT section underneath the contacts) but this issue clearly deserves a thorough microscopic analysis about the nature of the contacts. The conservation of the orbital quantum number seems more likely in the vertical quantum dots (VQD),[14] where the orbital quanutm number is the magnetic quantum number of the angular momentum.

Here, we take a different route and, assuming some degree of mixing in the orbital channel, ask ourselves about the robustness of the SU(4) Kondo effect against asymmetry in the couplings and/or mixing. The rest of the paper is organized as follows. In Sec. II we introduce the relevant model Hamiltonian and classify different schemes of lead-dot couplings. These different coupling schemes result in different symmetries and hence affect significantly the underlying Kondo physics. These effects are analyzed in the subsequent sections. We start our analysis with two renomalization group approaches in Sec. III. In Sec. IV two slave-boson approaches complement the previous results. Section V concludes the paper.

## II. MODEL

### A. Nearly degenerate localized orbitals

We consider a QD with two (nearly) degenerate localized orbitals which is coupled to reservoirs. As we mentioned before, we have in mind the experimental setup of Ref. 9 where a highly symmetric Kondo effect was demonstrated in a CNT QD. However, our description could well apply to vertical quantum dot (VQD),[14] where the orbitals correspond to two degenerate Fock-Darwin states with different values of the angular momentum quantum number. Hereafter we will denote this orbital quantum number by $m=1,2$. The dot is then described by the Hamiltonian

$$H_D = \sum_{m=1,2} \sum_{\sigma=\uparrow,\downarrow} \epsilon_{m\sigma} d^\dagger_{m\sigma} d_{m\sigma} + \sum_{(m,\sigma)\neq(m',\sigma')} U_{mm'} n_{m\sigma} n_{m'\sigma'}, \tag{1a}$$

where $\epsilon_{m\sigma}$ is the single-particle energy level of the localized state with orbital $m$ and spin $\sigma$, $d^\dagger_{m\sigma}$ ($d_{m\sigma}$) the fermion creation (annihilation) operator of the state, $n_{m\sigma}=d^\dagger_{m\sigma}d_{m\sigma}$ the occupation, $U_{mm}$ ($m=1,2$) the intraorbital Coulomb interaction, and $U_{12}$ the interorbital Coulomb interaction. The effect of the external magnetic field parallel to the symmetry axis of the system is to lifting the orbital and spin degeneracy of the single-particle energy levels. We will denote them by $\Delta_{\text{orb}}$ and $\Delta_Z$, respectively, so that the single-particle energy levels $\epsilon_{m\sigma}$ have the form

$$\epsilon_{m\sigma} = \epsilon_0 + \Delta_{\text{orb}}(\delta_{m,1} - \delta_{m,2}) + (\Delta_Z/2)(\delta_{\sigma,\uparrow} - \delta_{\sigma,\downarrow}). \tag{1b}$$

The precise values of the Coulomb interactions $U_{mm'}$ depend on the details of the system, but should be of the order of the charging energy $E_C=e^2/2C$ with $C$ being the total capacitance of the dot. In this work we focus on the regime where the system of the localized levels is occupied by a single electron ($\Sigma_{m\sigma}\langle n_{m\sigma}\rangle \approx 1$, quarter filling[15]) and the Coulomb interaction energy ($U_{mm'} \sim E_C$) is much bigger than other energy scales. In this regime the Hamiltonian in Eq. (1a) suffices to describe all relevant physics of our concern.

### B. Coupling schemes

Kondo physics arises as a result of the interplay between the strong correlation in the dot and the coupling of the localized electrons with the itinerant electrons in conduction bands. Naturally, different Kondo effects are observed depending on the way the dot is coupled to the electrodes and whether the orbital quantum number $m$ is conserved or not. Nevertheless, it turns out highly nontrivial experimentally to distinguish those different Kondo effects. In subsequent sections we will consider different coupling shemes between the dot and the electrodes, show how different physics emerges, and propose how to distinguish them umambiguously in experiments.

The two leads $\alpha=L$ and $R$ are treated as noninteracting gases of fermions

$$H_\alpha = \sum_k \sum_{\mu=1,2} \sum_\sigma \epsilon_{\alpha k\mu} a^\dagger_{\alpha k\mu\sigma} a_{\alpha k\mu\sigma}, \tag{1c}$$

where $\mu$ denotes the channels in the leads. Without loss of generality, we assume that there are two distinguished (groups of) channels $\mu=1$ and 2 in each lead. When the leads bears the same symmetry as the dot, this channel quantum number $\mu$ in the leads is identical to the orbital quantum number $m$ in the dot and will be preserved over the tunneling of electrons from the dot to leads and vice versa; see Fig. 1(a). Otherwise, the orbital channels become mixed; see Fig. 1(a). The most general situation is described by the tunneling Hamiltonian

$$H_T = \sum_{\alpha k\mu\sigma} (V_{\alpha k\mu m\sigma} a^\dagger_{\alpha k\mu\sigma} d_{m\sigma} + \text{H.c.}). \tag{1d}$$

The total Hamiltonian is then given by $H=H_L+H_R+H_T+H_D$.

For the sake of simplicity, we will assume identical electrodes ($\epsilon_{Lk\mu}=\epsilon_{Rk\mu}$), symmetric tunneling juctions ($V_{Lk\mu m\sigma}=V_{Rk\mu m\sigma}$). For simplicity, we ignore their $k$- and $\sigma$-dependence of the tunneling amplitudes. Therefore, we consider a simplified model with $V_{\alpha k\mu m\sigma}=V_{\mu,m}/\sqrt{2}$ which defines the widths

$$\Gamma_m \equiv \Gamma_{mm}, \quad \Gamma_{mm'} = \pi\rho_0 V^*_m V_{m'}, \tag{2}$$

where $\rho_0$ is the density of states in the reservoirs. Then in equilibrium the Hamiltonian $H$ in Eq. (1) is equivalent to $H=H_C+H_T+H_D$ with

$$H_C = \sum_{k\mu\sigma} \varepsilon_{k\mu} c^\dagger_{k\mu\sigma} c_{k\mu\sigma}, \tag{3a}$$

$$H_T = \sum_{k\mu,m,\sigma} (V_{\mu m} c^\dagger_{k\mu\sigma} d_{m\sigma} + \text{H.c.}), \tag{3b}$$

where we have made the canonical transformation

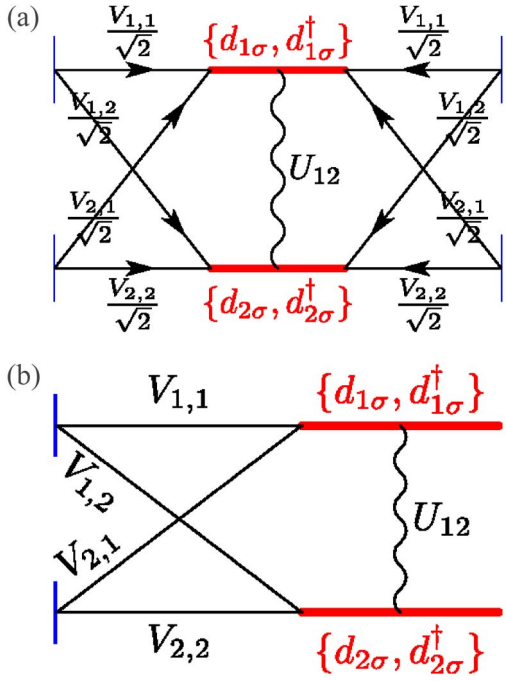


FIG. 1. (Color online) Schematic of a representative mesoscopic system in question. In (a) each of the two leads $L$ and $R$ has two conduction bands (or "modes") 1 and 2. The model with two leads in (a) is equivalent in equilibrium to the model in (b) with only one lead. The operators $c_{k\mu\sigma}$ ($\mu=1,2$ and $\sigma=\uparrow,\downarrow$) are related to $a_{Lk\mu\sigma}$ and $a_{Rk\mu\sigma}$ by the canonical tranformation in Eq. (4). The wiggly lines indicate the interorbital Coulomb interaction $U_{12}$ [the intraorbital itneraction $U_{mm}$ ($m=1,2$) is not shown].

$$c_{k\mu\sigma} = \frac{(a_{Lk\mu\sigma} + a_{Rk\mu\sigma})}{\sqrt{2}},$$

$$b_{k\mu\sigma} = \frac{(a_{Lk\mu\sigma} - a_{Rk\mu\sigma})}{\sqrt{2}}, \tag{4}$$

and discarded the decoupled term $\epsilon_{k\mu} b_{k\mu\sigma}^{\dagger} b_{k\mu\sigma}$.

In the following sections we investigate the physics described by the Hamiltonian in Eq. (3) and, in particular, clarify the role of index conservation in the symmetry of the underlying Kondo regime at low temperatures. In order to do this analysis we use four different approaches, the scaling theory (perturbative renormalization group approach), the renormalization group method (NRG), the slave-boson mean-field (SBMF) theory, and the noncrossing approximation (NCA).

## III. RENORMALIZATION GROUP APPROACHES

The renormalization group theory provides a convenient and powerful method to study low-energy properties of strongly correlated electron systems. Here we will take two RG approaches, the scaling theory[16–18] and the NRG method.[19–22] While the scaling theory is useful for a qualitative understanding of the model, a more precise quantitative analysis requires the use of more sophisticated methods like the NRG method. This method is known to be one of the most accurate and powerful theoretical tools to study quantum impurity problems (see Appendix A).

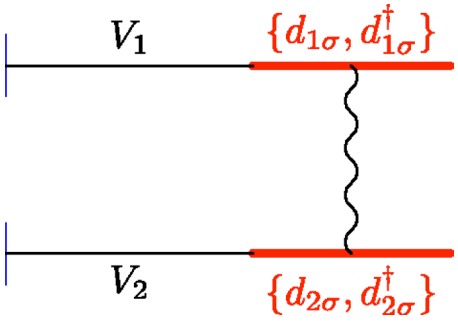


FIG. 2. (Color online) Schematics of the SU(4)-symmetric Anderson model.

### A. SU(4) Kondo effect

We now turn to the case where tunneling processes conserve the orbital quantum number; see Fig. 2. In this case, the Hamiltonian reads

$$H = \sum_{\alpha=L,R} \sum_{m=1,2} \sum_{k\sigma} \varepsilon_{\alpha k} a_{\alpha k m\sigma}^{\dagger} a_{\alpha k m\sigma} + \sum_{\alpha k m\sigma} V_m (a_{\alpha k m\sigma}^{\dagger} d_{m\sigma} + d_{m\sigma}^{\dagger} a_{\alpha k m\sigma}) + H_D \tag{5}$$

or [see Eqs. (3a) and (3b)]

$$H = \sum_{k m\sigma} \epsilon_k c_{k m\sigma}^{\dagger} c_{k m\sigma} + \sum_{k m\sigma} V_m (c_{k m\sigma}^{\dagger} d_{m\sigma} + d_{m\sigma}^{\dagger} c_{k m\sigma}) + H_D, \tag{6}$$

$$V_m \equiv V_{m,m}.$$

From the RG point of view, starting initially with nearly degenerate levels, all the localized levels are relevant for the spin and orbital fluctuations, and, as we will see below, contribute to the Kondo effect. To investigate the low-energy properties of the orbital and spin fluctuations of the model, we perform a Schrieffer-Wolf transformation and obtain an effective Kondo-type Hamiltonian

$$H = \sum_{k m\sigma} \epsilon_k c_{k m\sigma}^{\dagger} c_{k m\sigma} + H_{\text{eff}}^{\text{SU(4)}} - \Delta_Z S^z - 2\Delta_{\text{orb}} T^z - \frac{(\sqrt{J_1} - \sqrt{J_2})^2}{2} (1 + 4\mathbf{s}\cdot\mathbf{S})(t^x T^x + t^y T^y) + (J_1 - J_2)(\mathbf{s}\cdot\mathbf{S})(t^z + T^z), \tag{7}$$

where

$$H_{\text{eff}}^{\text{SU(4)}} = \frac{J_1 + J_2}{2} \{\mathbf{s}\cdot\mathbf{S} + \mathbf{t}\cdot\mathbf{T} + 4(\mathbf{s}\cdot\mathbf{S})(\mathbf{t}\cdot\mathbf{T})\}. \tag{8}$$

The exchange coupling constants $J_m$ ($m=1,2$) are given by

$$J_m = V_m^2 \left( \frac{1}{E_+} + \frac{1}{E_-} \right). \tag{9}$$

We note that the Kondo-type effective Hamiltonian in Eq. (7) is reduced to the SU(4)-symmetric Kondo model when $V_1$

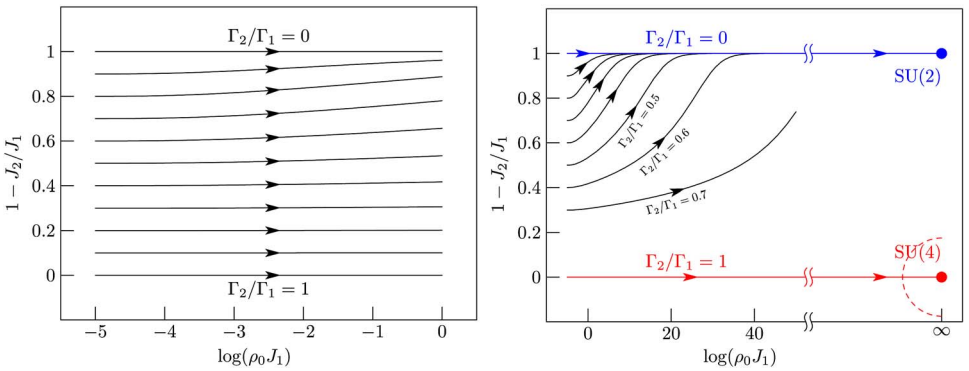


FIG. 3. (Color online) RG flows for different values of $\Gamma_2/\Gamma_1$ with $\Gamma_1$ fixed.

$=V_2$ and $\epsilon_{1\sigma}=\epsilon_{2\sigma}$. In this case, the orbitals play exactly the same role as the spins; orbitals are not distinguished from the spins.

Under the RG transformations reducing subsequently the conduction band width $D$ by $\delta D$, the Kondo-type effective Hamiltonian evolves into a generic form

$$H_{\text{eff}} = H_{\text{leads}} - \Delta_Z S^z - 2\Delta_{\text{orb}} T^z + 2J_1(\mathbf{s}\cdot\mathbf{S})\left(\frac{1}{2}+t^z\right)\left(\frac{1}{2}+T^z\right) + 2J_2(\mathbf{s}\cdot\mathbf{S})\left(\frac{1}{2}-t^z\right)\left(\frac{1}{2}-T^z\right) + \frac{1}{2}[J_4 + 4J_3(\mathbf{s}\cdot\mathbf{S})](t^+T^- + t^-T^+) + J_5 t^z T^z. \tag{10}$$

The level splitting $\Delta_{\text{orb}}$ and $\Delta_Z$ remain constant under the RG transformation

$$\frac{d\Delta_Z}{d\ln D} = \frac{d\Delta_{\text{orb}}}{d\ln D} = 0. \tag{11}$$

The exchange coupling constants $J_i$ $(i=1,\ldots,5)$ are initially given by Eq. (9) and by

$$J_3 = J_4 = \sqrt{J_1 J_2}, \quad J_5 = (J_1+J_2)/2. \tag{12}$$

Under the RG transformations, they scale as

$$\frac{dJ_1}{\rho_0 d\ln D} = -2J_1^2 - J_3(J_3+J_4), \tag{13a}$$

$$\frac{dJ_2}{\rho_0 d\ln D} = -2J_2^2 - J_3(J_3+J_4), \tag{13b}$$

$$\frac{dJ_3}{\rho_0 d\ln D} = -J_3(J_1+J_2+J_5) - J_4(J_1+J_2)/2, \tag{13c}$$

$$\frac{dJ_4}{\rho_0 d\ln D} = -3J_3(J_1+J_2)/2 - J_4 J_5, \tag{13d}$$

$$\frac{dJ_5}{\rho_0 d\ln D} = -3J_3^2 - J_4^2 \tag{13e}$$

for $D \gg \Delta_{\text{orb}} \gg \Delta_Z$. For $D \ll \Delta_{\text{orb}}$, it is clear from Eq. (10) that the orbital fluctuations are frozen and only $J_1$ is relevant, which scales as

$$\frac{dJ_1}{\rho_0 d\ln D} = -2J_1^2. \tag{14}$$

It implies that we recover the single-level Anderson model for $D \ll \Delta_{\text{orb}}$. Therefore in the remainder of this section, we will focus on the case $D \gg \Delta_{\text{orb}}$.

It is convenient to define the reduced variables $j_i \equiv J_i/J_1$ $(i=2,\ldots,5)$ and rewrite the RG equations (13) as

$$\frac{dj_2}{dx} = -j_2 + \frac{2j_2^2 + j_3(j_3+j_4)}{2+j_3(j_3+j_4)}, \tag{15a}$$

$$\frac{dj_3}{dx} = -j_3 + \frac{j_3(1+j_2+j_5) + j_4(1+j_2)/2}{2+j_3(j_3+j_4)}, \tag{15b}$$

$$\frac{dj_4}{dx} = -j_4 + \frac{3j_3(1+j_2)/2 + j_4 j_5}{2+j_3(j_3+j_4)}, \tag{15c}$$

$$\frac{dj_5}{dx} = -j_5 + \frac{3j_3^2 + j_4^2}{2+j_3(j_3+j_4)} \tag{15d}$$

with $x=\ln(\rho_0 J_1)$. $J_1$ obeys the scaling equation

$$\frac{1}{(\rho_0 J_1)^2}\frac{d(\rho_0 J_1)}{d\ln D} = -2 - j_3(j_3+j_4). \tag{16}$$

The RG equations (15) have two fixed points: one describing the SU(4) Kondo physics

$$j_2 = j_3 = j_4 = j_5 = 1 \tag{17}$$

and the other describing the usual SU(2) Kondo physics

$$j_2 = j_3 = j_4 = j_5 = 0, \tag{18}$$

both with $J_1=\infty$ as indicated in Fig. 3. Linearizing the RG equations (15) around the fixed points, one can easily show that both the SU(2) and SU(4) Kondo fixed points are stable fixed points [there is one marginal parameter at the SU(4) fixed point]. However, as indicated as a dashed semicircle in Fig. 3(b) the radius of convergence is finite while the fixed point itself is located at infinity. This implies that in principle, the SU(4) Kondo fixed point cannot be reached for arbitrarily small values of $1-\Gamma_2/\Gamma_1$. However, as illustrated in Fig. 3(a), in the region of physical interest for sufficiently small values of $1-\Gamma_2/\Gamma_1$, the scaling behavior is essentially governed by the SU(4) Kondo fixed point (see also Fig. 5).

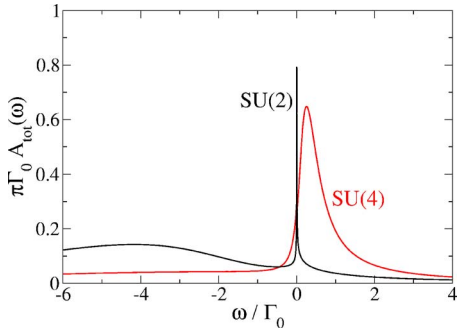


FIG. 4. (Color online) Comparison of the SU(2) and SU(4) Kondo model.

More importantly, for sufficiently small values of $1-\Gamma_2/\Gamma_1$, the SU(2) fixed point governs the physics only at extremely low energies. This suggests that the SU(4) Kondo signature can be observed exclusively at relatively higher energy scales (of order of the Kondo temperature), as in the recently reported experiment.[9]

At $B_\parallel=0$ and $\Gamma_1=\Gamma_2\equiv\Gamma_0$, the RG equations (13) reduce to a single equation

$$\frac{dJ_1}{\rho_0 d\ln D} = -4J_1^2. \tag{19}$$

Comparing this with the corresponding equation Eq. (14) for the usual single-level Anderson model, we note that the Kondo temperature is enhanced exponentially:

$$T_K^{\mathrm{SU}(4)} \sim \exp(-1/4\rho_0 J_1), \tag{20}$$

with respect to the SU(2) Kondo temperature

$$T_K^{\mathrm{SU}(2)} \sim \exp(-1/2\rho_0 J_1). \tag{21}$$

The perturbative RG analysis discussed above, whose validity is guaranteed only for $\rho_0 J_i \ll 1$, turns out to be qualitatively correct in a wide region of the parameter space and provides a clear interpretation of the model. To confirm the perturbative RG analysis and make quantitative analysis we used the NRG method (see the Appendix). Our NRG results are summarized in Figs. 4 and 5 where the *total* spectral density

$$A_d(E) = \sum_\sigma \sum_{mm'} \pi\Gamma_{mm'} A_{m'm;\sigma}(E), \tag{22}$$

which gives a direct information of the linear conductance,[23] is plotted.

The spectral density shows a peak near the Fermi energy, corresponding to the formation of the SU(4) Kondo state; see Fig. 4. The peak width, which is much broader than that for the SU(2) Kondo model (dotted line), demonstrates the exponential enhancement of the Kondo temperature mentioned above. Another remarkable effect is that the SU(4) Kondo peak shifts away from $\omega=E_F=0$ and is pinned at $\omega\approx T_K^{\mathrm{SU}(4)}$. This can be understood from the Friedel sum rule[24] which, in this case, gives $\delta=\pi/4$ for the scattering phase shift at $E_F$. Accordingly, the linear conductance at zero temperature is given by $\mathcal{G}_0=4(e^2/h)\sin^2\delta=2e^2/h$. It is interesting to recall

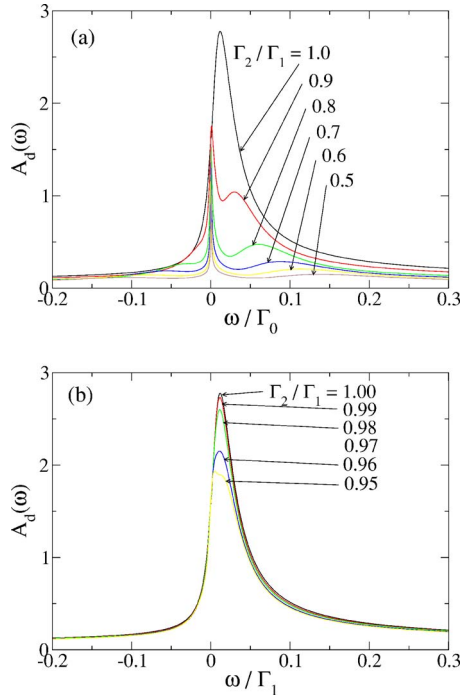


FIG. 5. (Color online) NRG results of the total spectral density $A_d(E)$ for different values of coupling asymmetry $\Gamma_2/\Gamma_1$. We took $\epsilon_0=-0.8D$, $\Gamma_1=0.1D$, $U_{mm'}=8D$, and $\Delta_{\mathrm{orb}}=\Delta_Z=0$.

that the Friedel sum rule gives the same linear conductance also for the two-level SU(2) Kondo model. Thus, neither the enhancement of the Kondo temperature nor the linear conductance, can distinguish between the SU(4) and the two-level SU(2) Kondo effects. This can only be achieved by studying the influence of a parallel magnetic field in the nonlinear conductance, as shown in Ref. 9

### B. Effects of mixing of orbital quantum numbers

To examine the stability of the SU(4) Kondo phenomena against orbital mixing, we consider the model (see Fig. 6):

$$H = \sum_{k\sigma} \varepsilon_k c_{k\sigma}^\dagger c_{k\sigma} + \sum_{km\sigma} V_0(c_{km\sigma}^\dagger d_{m\sigma} + d_{m\sigma}^\dagger c_{km\sigma}) + \sum_{km\sigma} V_X(c_{k\bar{m}\sigma}^\dagger d_{m\sigma} + d_{m\sigma}^\dagger c_{k\bar{m}\sigma}) + H_D, \tag{23}$$

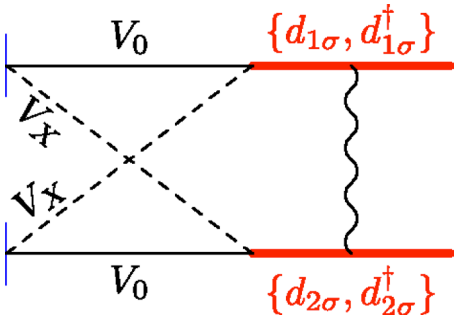


FIG. 6. (Color online) A model with finite mixing between orbital quantum numbers.

where the indexes in the Hamiltonian imply $\bar{1}=2$ and $\bar{2}=1$ and $V_0 \equiv V_{1,1}=V_{2,2}$ and $V_X \equiv V_{1,2}=V_{2,1}$. If we rewrite the Hamiltonian as

$$H = \sum_{k\sigma} \varepsilon_k c^\dagger_{k\sigma} c_{k\sigma} + \sum_{km\sigma} \{V_0 c^\dagger_{km\sigma} + V_X c^\dagger_{k\bar{m}\sigma}\} d_{m\sigma} + d^\dagger_{m\sigma}\{V_0 c_{km\sigma} + V_X c_{k\bar{m}\sigma}\} + H_D, \tag{24}$$

it now becomes clear that, in a pseudospin language, a finite amount of orbital mixing corresponds to having noncollinear leads with respect to the orbital "magnetization" axis which defines the pseudospin orientations $m=1$ and $m=2$ in the dot. In other words, each confined electron (with defined pseudospin) couples to a linear combination of pseudospin and, as a result, becomes rotated in pseudospin space by an angle defined by $\tan\phi = V_X/V_0$. Note that for the maximal mixing $V_X=V_0$, the tunneling electrons loose completely information about their pseudospin orientation. In this limit, one recovers the spin Kondo physics [SU(2) symmetry] of a two-level Anderson model [see next subsection, Eq. (36)]. For zero mixing $V_X=0$, the model reduces to the SU(4)-symmetric model of Eq. (6) (with tunnel amplitudes that do not depend on the orbital index).

After the RG transformation of the Anderson-type model in Eq. (23) until the single-particle energy levels are comparable with the conduction band width (when the charge fluctuations are suppressed), the SW transformation gives

$$H_{\rm eff} = \left(1 - \frac{J_X}{J_0}\right) H^{\rm SU(4)}_{\rm eff} + \frac{J_X}{J_0} H^{\rm SU(2)}_{\rm eff} + J_0 \sqrt{\frac{J_X}{J_0}} \times \left(1 - \sqrt{\frac{J_X}{J_0}}\right)(1 + 4\mathbf{s}\cdot\mathbf{S})(t^x + T^x) + 2J_X(t^x T^x), \tag{25}$$

where

$$H^{\rm SU(4)}_{\rm eff} = J_0\{\mathbf{s}\cdot\mathbf{S} + \mathbf{t}\cdot\mathbf{T} + 4(\mathbf{s}\cdot\mathbf{S})(\mathbf{t}\cdot\mathbf{T})\} \tag{26}$$

is the SU(4) Kondo model and

$$H^{\rm SU(2)}_{\rm eff} = 2J_0\mathbf{s}\cdot\mathbf{S}(1 + 2t^x)(1 + 2T^x) + J_0(t^x + T^x) \tag{27}$$

is the SU(2) Kondo model. The exchange coupling constants $J_0$ and $J_X$, respectively, are given by

$$J_0 = |V_0|^2\left(\frac{1}{E_+} + \frac{1}{E_-}\right), \quad J_X = |V_X|^2\left(\frac{1}{E_+} + \frac{1}{E_-}\right). \tag{28}$$

One can already grasp an idea about the effects of the mixing $J_X$ (i.e., $\Gamma_X$) of the orbital quantum numbers by considering the two limiting cases, $J_X=0$ (no mixing) and $J_X=J_0$ (maximal mixing), of the effective Hamiltonian (25). In the case of no mixing ($J_X=0$), the effective Hamiltonian (25) is reduced to the SU(4)-symmetric Kondo model Eq. (26), which was already discussed in the previous section. The Kondo temperature is $T_K \sim D\exp(-1/4J_0)$. When the mixing is maximal ($J_X=J_0$), on the other hand, the effective Hamiltonian becomes $H^{\rm SU(2)}_{\rm eff}$ in Eq. (27).

Under the RG procedures, the effective Hamiltonian (25) transforms in the general form

$$H_{\rm eff} = J_1\mathbf{s}\cdot\mathbf{S} + \{J_3(t^z T^z) + 4J_2(\mathbf{s}\cdot\mathbf{S})(t^z T^z)\} + \{J_4(t^x T^x + t^y T^y) + 4J_6(\mathbf{s}\cdot\mathbf{S})(t^x T^x + t^y T^y)\} + \{J_5(t^x T^x - t^y T^y) + 4J_7(\mathbf{s}\cdot\mathbf{S}) \times (t^x T^x - t^y T^y)\} + \{J_9 + 4J_8(\mathbf{s}\cdot\mathbf{S})(t^x + T^x)\}. \tag{29}$$

The exchange coupling constants are initially given by

$$J_1 = J_0 + J_X, \quad J_2 = J_3 = J_0 - J_x, \quad J_4 = J_6 = J_0,$$

$$J_5 = J_7 = J_X, \quad J_9 = J_8 = \sqrt{J_0 J_X}. \tag{30}$$

With the RG transformations, they scale as

$$\frac{dJ_1}{\rho_0 d\ln D} = -J_1^2 - J_2^2 - 2J_6^2 - 2J_7^2 - 8J_8^2, \tag{31a}$$

$$\frac{dJ_2}{\rho_0 d\ln D} = -2J_1J_2 - 2J_4J_6 + 2J_5J_7, \tag{31b}$$

$$\frac{dJ_3}{\rho_0 d\ln D} = -J_4^2 + J_5^2 - 3J_6^2 + 3J_7^2, \tag{31c}$$

$$\frac{dJ_4}{\rho_0 d\ln D} = -J_3J_4 - 3J_2J_6, \tag{31d}$$

$$\frac{dJ_5}{\rho_0 d\ln D} = J_3J_5 + 3J_2J_7, \tag{31e}$$

$$\frac{dJ_6}{\rho_0 d\ln D} = -J_2J_4 - 2J_1J_6 - J_3J_6 - 4J_8^2, \tag{31f}$$

$$\frac{dJ_7}{\rho_0 d\ln D} = J_2J_5 - 2J_1J_7 + J_3J_7 - 4J_8^2, \tag{31g}$$

$$\frac{dJ_8}{\rho_0 d\ln D} = -2J_1J_8 - 2J_6J_8 - 2J_7J_8, \tag{31h}$$

and

$$\frac{dJ_9}{d\ln D} = 0. \tag{32}$$

As before [see Eq. (15)], it is convenient to work with the reduced coupling constants $j_i \equiv J_i/J_1$. In terms of the reduced exchange coupling constants, the RG equations read

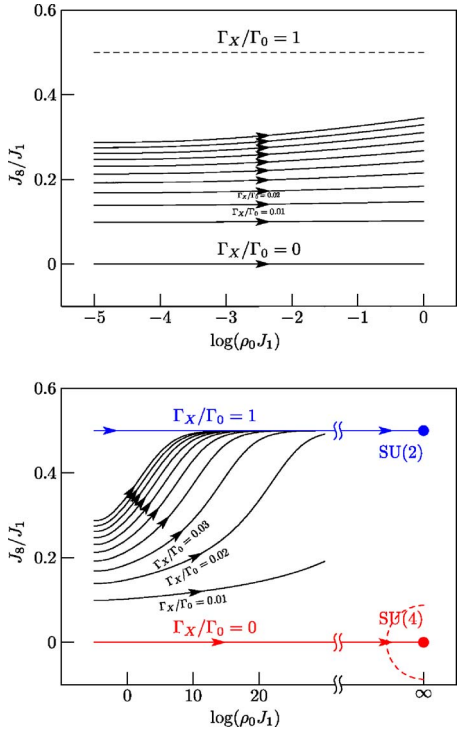


FIG. 7. (Color online) The RG flow in the case where there is a finite mixing of the orbital quantum numbers $m$.

$$\frac{dj_2}{dx} = -j_2 + \frac{2j_2 + 2j_4j_6 - 2j_5j_7}{1 + j_2^2 + 2j_6^2 + 2j_7^2 + 8j_8^2}, \tag{33a}$$

$$\frac{dj_3}{dx} = -j_3 + \frac{j_4^2 - j_5^2 + 3j_6^2 - 3j_7^2}{1 + j_2^2 + 2j_6^2 + 2j_7^2 + 8j_8^2}, \tag{33b}$$

$$\frac{dj_4}{dx} = -j_4 + \frac{j_3j_4 + 3j_2j_6}{1 + j_2^2 + 2j_6^2 + 2j_7^2 + 8j_8^2}, \tag{33c}$$

$$\frac{dj_5}{dx} = -j_5 - \frac{j_3j_5 + 3j_2j_7}{1 + j_2^2 + 2j_6^2 + 2j_7^2 + 8j_8^2}, \tag{33d}$$

$$\frac{dj_6}{dx} = -j_6 + \frac{j_2j_4 + 2j_6 + j_3j_6 + 4j_8^2}{1 + j_2^2 + 2j_6^2 + 2j_7^2 + 8j_8^2}, \tag{33e}$$

$$\frac{dj_7}{dx} = -j_7 - \frac{j_2j_5 - 2j_7 + j_3j_7 - 4j_8^2}{1 + j_2^2 + 2j_6^2 + 2j_7^2 + 8j_8^2}, \tag{33f}$$

$$\frac{dj_8}{dx} = -j_8 + \frac{2j_8 + 2j_6j_8 + 2j_7j_8}{1 + j_2^2 + 2j_6^2 + 2j_7^2 + 8j_8^2} \tag{33g}$$

together with

$$\frac{1}{(\rho_0 J_1)^2}\frac{d(\rho_0 J_1)}{d\ln D} = -(1 + j_2^2 + 2j_6^2 + 2j_7^2 + 8j_8^2). \tag{34}$$

The RG equations (33) again have two fixed points, one associated with the SU(2) Kondo effects and the other with the SU(4) Kondo effects; see Fig. 7. The RG flow diagram in Fig. 7 is reminiscent of that in Fig. 3. Both fixed points are stable. However, since the radius of convergence of the SU(4) Kondo fixed point is finite, the SU(4) Kondo fixed point cannot be reachable even for arbitrarily small mixing $V_X$; Fig. 7(b). However, in the region of physical interest, the physics is essentially governed by the SU(4) Kondo fixed point for sufficiently small $V_X$; Fig. 7(a). Therefore, the SU(4) Kondo physics is in principle unstable against both the orbital quantum number anisotropy $1-\Gamma_2/\Gamma_1$ and the orbital mixing $\Gamma_X$. For sufficiently small values of those, however, the SU(4) Kondo physics still determines the transport properties except at extremely low energy scales. As we mentioned earlier, this suggests that to observe the indications of the SU(4) Kondo physics *exclusively* one has to investigate the properties at relatively higher energies (order of Kondo temperature). This is confirmed and demonstrated in the NRG results summarized in Fig. 8. We will also see below that there is no way to distinguish the two-level SU(2) Kondo physics and the SU(4) Kondo physics experimentally by means of linear conductance.

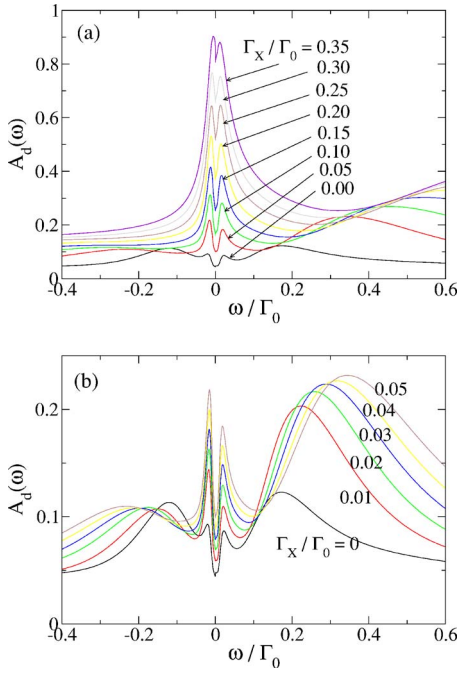


FIG. 8. (Color online) NRG results on the effects of the finite mixing of the orbital quantum number $m$. We took $\epsilon_0 = -0.8D$, $\Gamma_0 = 0.08D$, $U_{mm'} = 8D$, $\Delta_{\rm orb} = 32T_K^{\rm SU(4)}$, and $\Delta_Z = 2T_K^{\rm SU(4)}$.

### C. Two-level SU(2) Kondo effect

As we have mentioned in the previous subsection, at maximum mixing $V_0 = V_X$ the physics becomes that of a two-level SU(2) Anderson model (see Fig. 9). In this case, the only degree of freedom that is conserved during tunneling is spin and the total Hamiltonian reads

$$H = \sum_{\alpha=L,R}\sum_{k\sigma}\varepsilon_{\alpha k}a^\dagger_{\alpha k\sigma}a_{\alpha k\sigma} + \sum_{\alpha k m\sigma} V_m(a^\dagger_{\alpha k\sigma}d_{m\sigma} + d^\dagger_{m\sigma}a_{\alpha k\sigma}) + H_D \tag{35}$$

or, equivalently [see Eq. (4)],

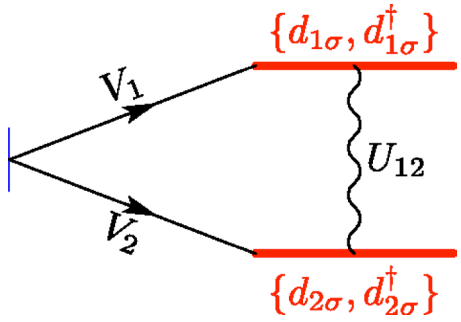


FIG. 9. (Color online) Schematic of the two-level SU(2)-symmetric Anderson model.

$$H = \sum_{k\sigma} \varepsilon_k c_{k\sigma}^{\dagger} c_{k\sigma} + \sum_{km\sigma} V_m (c_{k\sigma}^{\dagger} d_{m\sigma} + d_{m\sigma}^{\dagger} c_{k\sigma}) + H_D. \quad (36)$$

As the scaling theory of the Kondo-type Hamiltonian obtained from the two-level Anderson model has been developed in detail in Refs. 25 and 26, here we will focus on the first stage, which highlights the difference between the two-level SU(2)-symmetric Anderson model and the SU(4)-symmetric Anderson model. Finally, the physical arguments based on the perturbative RG theory will be examined quantitatively by means of the NRG method.

As we integrate out the electronic states in the ranges $[-D,-(D-\delta D)]$ and $[D-\delta D, D]$ of the conduction band, the dot Hamiltonian (1a) evolves as

$$H_D = \sum_{m\sigma} \epsilon_{m\sigma} d_{m\sigma}^{\dagger} d_{m\sigma} - t \sum_{\sigma} (d_{1\sigma}^{\dagger} d_{2\sigma} + d_{2\sigma}^{\dagger} d_{1\sigma}) + \sum_{(m,\sigma)\neq(m',\sigma')} U_{mm'} n_{m\sigma} n_{m'\sigma'} \quad (37)$$

with other terms in the total Hamiltonian (36) kept unchanged. Notice here the appearance of the new term in $t$, i.e., a direct transition between the two orbitals $m=1$ and 2. The scaling of the parameters $\epsilon_{m\sigma}$ and $t$ are governed by the RG equations

$$\frac{d\epsilon_{m\sigma}}{d \ln D} = -\frac{2}{\pi} \Gamma_m \quad (38)$$

and

$$\frac{dt}{d \ln D} = -\frac{2}{\pi} \sqrt{\Gamma_1 \Gamma_2}, \quad (39)$$

respectively.

The RG equation (38) for the single-particle energy levels $\epsilon_{m\sigma}$ is the same as in the usual single-level Anderson model[17,18] (the corresponding RG flow diagram is shown in Fig. 10). However, due to the direct transition $t$ emerging from the RG equation (39), $\epsilon_{m\sigma}$ are not relevant to the Kondo effect [they are not the eigenvalues of $H_D$ in Eq. (37)]. To find the relevant energy level(s) that is (are) directly involved in the Kondo effect, one can diagonalize $H_D$ in Eq. (37) by means of the canonical tranformation

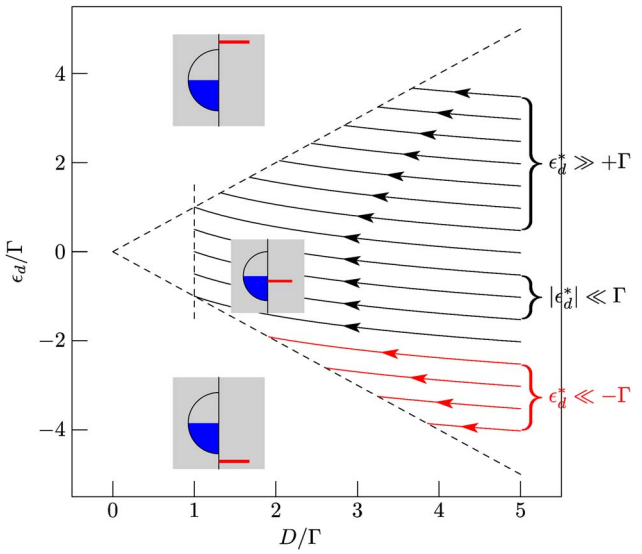


FIG. 10. (Color online) Scaling of the single-particle energy level $\epsilon_d$, to be compared with $\epsilon_{m\sigma}$ in Eq. (38), of the single-level Anderson model. $\epsilon_d^* = \epsilon_d(D=\Gamma)$ is the scale-invariant quantity.

$$\begin{bmatrix} d_{+,\sigma} \\ d_{-,\sigma} \end{bmatrix} = \begin{bmatrix} \cos(\theta/2) & \sin(\theta/2) \\ -\sin(\theta/2) & \cos(\theta/2) \end{bmatrix} \begin{bmatrix} d_{1\sigma} \\ d_{2\sigma} \end{bmatrix}, \quad (40)$$

where the angle $\phi$ is defined by the relation

$$\tan\theta \equiv \frac{t}{\epsilon_2 - \epsilon_1}. \quad (41)$$

The dot Hamiltonian in Eq. (37) is then rewritten as

$$H_D = \sum_{\mu=\pm} \sum_{\sigma} \epsilon_{\mu} d_{\mu\sigma}^{\dagger} d_{\mu\sigma} + \sum_{(m,\sigma)\neq(m',\sigma')} U_{mm'} n_{m\sigma} n_{m'\sigma'}, \quad (42)$$

with

$$\epsilon_{\mu=\pm} = \frac{1}{2}(\epsilon_1 + \epsilon_2) \mp \frac{1}{2}\sqrt{(\epsilon_1 - \epsilon_2)^2 + t^2}. \quad (43)$$

At the same time, the canonical transformation in Eq. (40) also changes the coupling term in the total Hamiltonian (36) to

$$H_T = \sum_{\mu=\pm} \sum_{k\sigma} V_{\mu} (c_{k\sigma}^{\dagger} d_{\mu\sigma} + d_{\mu\sigma}^{\dagger} c_{k\sigma}) \quad (44)$$

with $V_{\pm}$ defined by

$$\begin{bmatrix} V_+ \\ V_- \end{bmatrix} = \begin{bmatrix} \cos(\theta/2) & \sin(\theta/2) \\ -\sin(\theta/2) & \cos(\theta/2) \end{bmatrix} \begin{bmatrix} V_1 \\ V_2 \end{bmatrix}. \quad (45)$$

Accordingly, the tunneling rates $\Gamma_{\pm} \equiv \pi\rho_0 |V_{\pm}|^2$ of the effective orbital levels $\epsilon_{\pm,\sigma}$ are given by

$$\Gamma_{\pm} = \frac{1}{2}(\Gamma_1 + \Gamma_2) \pm \sqrt{\Gamma_1 \Gamma_2} \sin\theta + \frac{1}{2}(\Gamma_1 - \Gamma_2)\cos\theta. \quad (46)$$

Figure 11 shows the scaling of $\epsilon_{\pm}$ (the arrowed lines) and $\Gamma_{\pm}$ (the widths of the shadowed regions around $\epsilon_{\pm}$) governed by Eqs. (38), (39), (43), and (46). Note that the effective

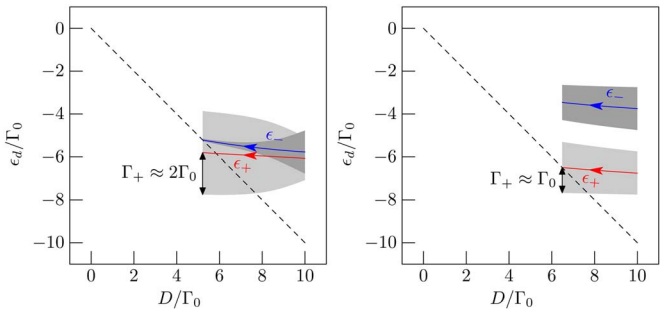


FIG. 11. (Color online) Scaling of the two-level SU(2)-symmetric Anderson model. The arrowed lines indicate the RG flow of the effective single-particle energy levels $\epsilon_\pm$ [see Eq. (43)] and the widths of the shadowed regions around $\epsilon_\pm$ the RG flow of $\Gamma_\pm$ [see Eq. (46)]. We have defined $\Gamma_0 \equiv (\Gamma_1+\Gamma_2)/2$.

single-particle energy levels $\epsilon_\pm$ always repel each other,[27] and the hybridization $\Gamma_+$ ($\Gamma_-$) of the lower (upper) level $\epsilon_+$ ($\epsilon_-$) always increases (decreases). Essential in this scaling property of the two-level Anderson model is the direct transition $t$ between the orbitals $m=1$ and 2 mediated by the conduction band.

The scaling of $\epsilon_\pm$ and $\Gamma_\pm$ stops when the lower level $\epsilon_+$ becomes comparable with $D$ ($\epsilon_+ \simeq D$); see Fig. 11. Then the charge fluctuations are highly suppressed and the occupation of the lower level is close to unity ($\langle n_+ \rangle \approx 1$). Therefore, only the lower level $\epsilon_+$ gets involved in the Kondo physics, and hence the resulting Kondo effect is identical to the usual SU(2) Kondo effect. To be more specific, let us consider the two limiting cases, $|\epsilon_1-\epsilon_2| \gg \Gamma_0$ and $|\epsilon_1-\epsilon_2| \ll \Gamma_0$, assuming

$$|\Gamma_1 - \Gamma_2| \ll \Gamma_0 \equiv (\Gamma_1 + \Gamma_2)/2. \tag{47}$$

Since $t \sim \Gamma_0$, one has

$$\theta \approx \begin{cases} \pi/2, & |\epsilon_1 - \epsilon_2| \ll \Gamma_0, \\ 0, & |\epsilon_1 - \epsilon_2| \gg \Gamma_0 \end{cases} \tag{48}$$

or, equivalently,

$$\Gamma_+ \approx \begin{cases} 2\Gamma_0, & |\epsilon_1 - \epsilon_2| \ll \Gamma_0, \\ \Gamma_0, & |\epsilon_1 - \epsilon_2| \gg \Gamma_0. \end{cases} \tag{49}$$

This implies that when the two orbital levels are nearly degenerate ($|\epsilon_1-\epsilon_2| \ll \Gamma_0$) the Kondo temperature[17,18] is enhanced exponentially,

$$T_K \simeq \frac{1}{2}\sqrt{2\Gamma_0 D}\exp\left[+\frac{\pi\epsilon_0}{2\Gamma_0}\right], \tag{50}$$

[with $\epsilon_0 \equiv (\epsilon_1+\epsilon_2)/2$] compared with the single-level case (i.e., $|\epsilon_1-\epsilon_2| \gg \Gamma_0$) with

$$T_K^0 \simeq \frac{1}{2}\sqrt{\Gamma_0 D}\exp\left[+\frac{\pi\epsilon_0}{\Gamma_0}\right]. \tag{51}$$

In the limit of nearly degenerate levels ($|\epsilon_1-\epsilon_2| \ll \Gamma_0$), the upper level $\epsilon_-$ is located at distance smaller than $\Gamma_+$ from the lower level $\epsilon_+$ [$(\epsilon_- - \epsilon_+) \lesssim \Gamma_+$ (see Fig. 11)] and the transition from $\epsilon_+$ to $\epsilon_-$ is allowed in general. Indeed, this effect can be taken into account by a proper SW transformation including

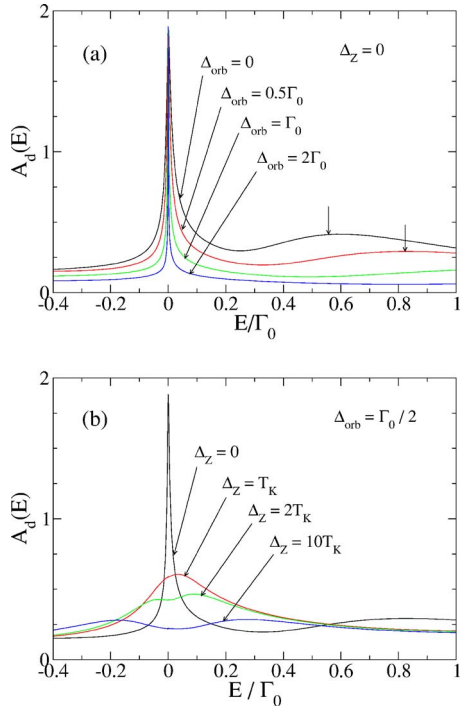


FIG. 12. (Color online) Total single-particle excitation spectrum $A_d(\omega)$ (a) with only the orbital degeneracy lifted ($\Delta_{orb} \neq 0$, $\Delta_Z = 0$) and (b) both the orbital and spin degeneracies lifted ($\Delta_{orb}, \Delta_Z \neq 0$). The short vertical arrows indicate the transition from $\epsilon_+$ to $\epsilon_-$, whose excitation energy is given by $\Delta_{eff}$ [see Eq. (52)]. We took $\epsilon_0 = -0.8D$, $\Gamma_0 = 0.1D$, and $U_{mm'} = 8D$.

both levels and the scaling of the resulting Kondo-like Hamiltonian,[25,26] and gives rise to a bump structure at $\omega = \Delta_{eff}$ above the Fermi energy $E_F$ of the leads, with $\Delta_{eff}$ given by[27] (with $\epsilon_{1\sigma} = \epsilon_{2\sigma}$ initially)

$$\Delta_{eff} \sim \frac{2\Gamma_0}{\pi}\ln\frac{D}{\Gamma_0}, \tag{52}$$

in the single-particle excitation spectrum $A_d(\omega)$ in Fig. 12; see below.

Again, all the interpretations made above based on the perturbative RG are confirmed with the NRG method. Figure 12 shows the total spectral density $A_d(E)$. One can see that as $\Delta_{orb}$ increases with $\Delta_Z = 0$, the Kondo peak gets sharper, i.e., the enhancement of the Kondo temperature $T_K$ in Eq. (50) diminishes for $\Delta_{orb} \gtrsim \Gamma_0$; see Fig. 12(a). Notice that the bump above the Fermi energy originates from the excitation via the transition from the lower level $\epsilon_+$ to the higher level $\epsilon_-$, and thus is located at $E = \Delta_{eff}$; see Eq. (52). When we allows $\Delta_Z$ finite as well, then the Kondo peak now splits into two because of the Zeeman splitting.[28,29]

## IV. SLAVE-BOSON TREATMENT

In order to confirm our previous results and obtain analytical expressions for intermediate mixing, we also use slave boson techniques. In particular, the SBMF approach, which is a good approximation in the strong coupling limit $T \ll T_K$, allows us to obtain analytical expressions for the Kondo tem-

perature and the Kondo peak position for arbitrary mixing. Our SBMFT results are complemented with a NCA, which takes into account both thermal and charge fluctuations in a self-consistent manner.

At equilibrium it is convenient to change to a representation in terms of the symmetric (even) and antisymmetric (odd) combinations of the localized and delocalized orbital channels.[30] Thus, the even-odd transformation consists of $a_{k,1(2),\sigma}=(c_{k_e\sigma}\pm ic_{k_o\sigma})\sqrt{2}$ and $d_{1(2)\sigma}=(d_{e\sigma}\pm id_{o\sigma})/\sqrt{2}$. The Hamiltonian [Eq. (3)] in this basis reads

$$H=\sum_{\sigma,\nu=e,o}\epsilon_{k_\nu}c^\dagger_{k_\nu,\sigma}c_{k_\nu,\sigma}+\sum_{\sigma,\nu=e,o}\varepsilon_{\nu\sigma}d^\dagger_{\nu,\sigma}d_{\nu,\sigma}+\sum_{\nu=e,o}Un_{\nu\downarrow}n_{\nu\uparrow}+Un_en_o+V_e\sum_{k_e,\sigma}(c^\dagger_{k_e,\sigma}d_{e\sigma}+\text{H.c.})+V_o\sum_{k_o,\sigma}(c^\dagger_{k_o,\sigma}d_{o\sigma}+\text{H.c.}),\tag{53}$$

where, again, we have considered $V_0=V_{1,1}=V_{2,2}$, $V_X=V_{1,2}=V_{2,1}$, $U_{m,m'}=U$, and $\varepsilon_{\nu,\sigma}=\varepsilon_{0,\sigma}$. The occupation per channel and spin is given by $n_{\nu\sigma}=d^\dagger_{\nu\sigma}d_{\nu\sigma}$ and the total occupation per channel is $n_\nu=\Sigma_\sigma n_{\nu\sigma}$. In Eq. (53) the tunneling amplitudes for each channel are: $V_e\equiv V_0+V_X$ and $V_o\equiv V_0-V_X$. In order to normalize the total tunneling rate we take for the diagonal and off-diagonal tunneling amplitude $V_0=V\cos\phi$ and $V_X=V\sin\phi$, namely, $V_e=V(\cos\phi+\sin\phi)$ and $V_o=V(\cos\phi-\sin\phi)$. Notice that $\phi\in[0,\pi/4]$ in order to always have $V_o$ positively defined. There are two very different situations, namely, (i) when $\phi=0$, where there are only tunneling processes that conserve the orbital index and (ii) when $\phi=\pi/4$ where the mixing and no mixing tunneling amplitudes are the same.

Now we write the physical fermionic operator as a combination of a pseudofermion and a boson operator as follows: $d_{\nu\sigma}=b^\dagger f_{\nu\sigma}$, where $f_{\nu,\sigma}$ is the pseudofermion that annihilates one "occupied state" in the $\nu$th localized orbital and $b^\dagger$ is a boson operator that creates an "empty state." Quite generally the intra(inter) Coulomb interaction is very large and we can safely take the limit of $U\to\infty$. This fact enforces the constraint $\Sigma_{\nu\sigma}f^\dagger_{\nu\sigma}f_{\nu\sigma}+b^\dagger b=1$, that prevents the accomodation of two electrons at the same time in either the same orbital or different orbitals. This constraint is treated with a Lagrange multiplier:

$$H_{\text{SB}}=\sum_{\sigma,\nu=e,o}\epsilon_{k_\nu}c^\dagger_{k_\nu,\sigma}c_{k_\nu,\sigma}+\sum_{\sigma,\nu=e,o}\varepsilon_{0,\sigma}f^\dagger_{\nu,\sigma}f_{\nu,\sigma}+\frac{\bar{V}_\nu}{\sqrt{N}}\sum_{k,\sigma,\nu=e,o}(c^\dagger_{k_\nu,\sigma}b^\dagger f_{\nu,\sigma}+\text{H.c.})+\lambda\left(\sum_{\nu,\sigma}f^\dagger_{\nu,\sigma}f_{\nu,\sigma}+b^\dagger b-1\right).\tag{54}$$

Notice that we have rescaled the tunneling amplitudes $V_{e(o)}\to\bar{V}_{e(o)}\sqrt{N}$ according to the spirit of a $1/N$ expansion ($N$ is the total degeneracy of the localized orbital).

Our next task is to solve this Hamiltonian, which is rather complicated due to the presence of the three operators in the tunneling part and the constraint. In order to do this we employ two approaches that describe two different physical regimes. The first one is the SBMFT approach, which describes properly the low-temperature strong coupling regime. This SBMFT is a good approximation in the deep Kondo limit, namely only spin fluctuations are taken into account. The NCA, on the other hand, takes into account both thermal and charge fluctuations in a self-consistent manner. It is well known that the NCA fails in describing the low-energy strong coupling regime. Nevertheless, the NCA has proven to give reliable results for temperatures down to a fraction of $T_K$.

### A. Slave-boson mean-field theory

We start discussing the mean-field approximation of Eq. (54). The merit of this approach is its simplicity while capturing the main physics of the pure Kondo regime. It has been successfully applied to investigate the out-of-equilibrium Kondo effect[31–34] and double quantum dots,[35–39] just to mention a few. This approach corresponds to the lowest order in the $1/N$ expansion, $\mathcal{O}(1)$ where the boson operator $b(t)$ is replaced by its classical (nonfluctuating) average, namely, $b(t)/\sqrt{N}\to\langle b\rangle/\sqrt{N}\equiv\tilde{b}$, thereby neglecting charge fluctuations. In the limit $N\to\infty$ this approximation is exact. Then the mean-field Hamiltonian is given by

$$H_{\text{MF}}=\sum_{\sigma,\nu=e,o}\epsilon_{k_\nu}c^\dagger_{k_\nu,\sigma}c_{k_\nu\sigma}+\sum_{\nu,\sigma}\tilde{\varepsilon}_{0,\sigma}f^\dagger_{\nu,\sigma}f_{\nu,\sigma}+\sum_{\nu,k,\sigma}(\tilde{V}_\nu c^\dagger_{\nu,k,\sigma}f_{\nu,\sigma}+\text{H.c.})+\lambda\left(\sum_{\nu,\sigma}f^\dagger_{\nu,\sigma}f_{\nu,\sigma}+N|\tilde{b}|^2-1\right),\tag{55}$$

where $\tilde{V}_\nu=\bar{V}_\nu\tilde{b}=V_\nu\langle b\rangle$ and $\tilde{\varepsilon}_{0,\sigma}=\varepsilon_{0,\sigma}+\lambda$ are the renormalized tunneling amplitude and renormalized orbital level. The two mean field parameters $\tilde{b}$ and $\lambda$ have to be determined through the mean-field equations. These equations are the constraint

$$\sum_{\nu,\sigma}\langle f^\dagger_{\nu,\sigma}(t)f_{\nu,\sigma}(t)\rangle+N|\tilde{b}|^2=1,\tag{56}$$

and the equation of motion (EOM) of the boson field

$$\sum_{\nu,k,\sigma}\tilde{V}_\nu\langle c^\dagger_{k_\nu\sigma}(t)f_{\nu,\sigma}(t)\rangle+\lambda N|\tilde{b}|^2=0.\tag{57}$$

Now we write these two equations in terms of nonequilibrium Green functions. The Green function for the $\nu$ localized orbital $(\nu\in e,o)$ $G^<_{\nu,\sigma}(t-t')=-i\langle f^\dagger_{\nu,\sigma}(t')f_{\nu,\sigma}(t)\rangle$, and the corresponding lesser lead-orbital Green function is $G^<_{\nu,\sigma,k_\nu\sigma}(t-t')=-i\langle c^\dagger_{k_\nu\sigma}(t')f_{\nu,\sigma}(t)\rangle$. Expressing the mean-field equations in terms of these nonequilibrium Green functions, (56) and (57) become

$$\sum_\sigma G^<_{\nu,\sigma}(t,t)+N|\tilde{b}|^2=1,\tag{58a}$$

$$\sum_{\nu,k,\sigma} \tilde{V}_\nu G^<_{\nu,\sigma;k_\nu\sigma}(t,t) + \lambda N|\tilde{b}|^2 = 0. \tag{58b}$$

In order to solve the set of mean field equations, we proceed as follows. First, we employ the analytic continuation rules to the EOM of the time-ordered Green's functions $G^t_{\nu,\sigma}(t-t') = -i\langle T_C\{f^\dagger_{\nu\sigma}(t')f_{\nu\sigma}(t)\}\rangle$ and $G^t_{\nu,\sigma;k_\nu\sigma}(t-t') = -i\langle T_C\{c^\dagger_{k_\nu\sigma}(t')f_{\nu,\sigma}(t)\}\rangle$ (where $T_C$ is the time-ordering operator along a complex time contour).[40] Second, we use the EOM technique to relate the lead-orbital Green function with the orbital Green function. And finally we rewrite the mean-field equations in the frequency domain (we take $\varepsilon_{0,\sigma}=\varepsilon_0$)

$$|\tilde{b}^2| - \frac{1}{N}\sum_{\nu,\sigma}\int \frac{d\epsilon}{2\pi i} G^<_{\nu\sigma}(\epsilon) = \frac{1}{N}, \tag{59a}$$

$$\lambda|\tilde{b}|^2 + \frac{1}{N}\sum_{\nu,\sigma}\int \frac{d\epsilon}{2\pi i} G^<_{\nu\sigma}(\epsilon)(\varepsilon_0 - \tilde{\varepsilon}_0) = 0. \tag{59b}$$

The integrals appearing in Eq. (59) can be performed analytically by using a Lorentzian cutoff $\rho(\epsilon)=D/(\epsilon^2+D^2)$ for the DOS in the leads and the lesser orbital Green function $G^<_\nu(\epsilon)=2i\tilde{\Gamma}_\nu f(\epsilon)/[(\epsilon-\tilde{\varepsilon}_0)^2+\tilde{\Gamma}^2_\nu]$ [$f(\epsilon)$ is the Fermi distribution function]

$$\frac{2}{\pi N}\,\mathrm{Im}\left[\ln\left(\frac{\tilde{\varepsilon}_0 + i\tilde{\Gamma}_e}{D}\right)\right] + \frac{2}{\pi N}\,\mathrm{Im}\left[\ln\left(\frac{\tilde{\varepsilon}_0 + i\tilde{\Gamma}_o}{D}\right)\right] = \frac{1}{N} - |\tilde{b}|^2, \tag{60a}$$

$$\frac{2\tilde{\Gamma}_e}{\pi N}\,\mathrm{Re}\left[\ln\left(\frac{\tilde{\varepsilon}_0 + i\tilde{\Gamma}_e}{D}\right)\right] + \frac{2\tilde{\Gamma}_o}{\pi N}\,\mathrm{Re}\left[\ln\left(\frac{\tilde{\varepsilon}_0 + i\tilde{\Gamma}_o}{D}\right)\right] = -\lambda|\tilde{b}|^2, \tag{60b}$$

where $\tilde{\Gamma}_{e(o)}=\bar{\Gamma}_{e(o)}|\tilde{b}|^2$. In the deep Kondo limit, namely, $\frac{1}{N} - |\tilde{b}|^2 \approx \frac{1}{N}$ and $-\lambda \approx \varepsilon_0$, these equations can be written as

$$\mathrm{Im}\left[\ln\left(\frac{\tilde{\varepsilon}_0 + i\tilde{\Gamma}_e}{D}\right)\right] + \mathrm{Im}\left[\ln\left(\frac{\tilde{\varepsilon}_0 + i\tilde{\Gamma}_o}{D}\right)\right] = \frac{\pi}{2}, \tag{61a}$$

$$\Gamma_e\,\mathrm{Re}\left[\ln\left(\frac{\tilde{\varepsilon}_0 + i\tilde{\Gamma}_e}{D}\right)\right] + \Gamma_o\,\mathrm{Re}\left[\ln\left(\frac{\tilde{\varepsilon}_0 + i\tilde{\Gamma}_o}{D}\right)\right] = \frac{\pi\varepsilon_0}{2}, \tag{61b}$$

where $\Gamma_{e(o)}=\bar{\Gamma}_{e(o)}/N$ are the original rates. Using the parametrization $V_e=V(\cos\phi+\sin\phi)$ and $V_o=V(\cos\phi-\sin\phi)$, the tunneling rates read $\Gamma_e=\pi V^2\rho(1+\sin 2\phi)=\Gamma(1+\sin 2\phi)$ and $\Gamma_o=\rho=\pi V^2\rho(1-\sin 2\phi)=\Gamma(1-\sin 2\phi)$. Taking $\sin 2\phi=\beta$, with $\beta\in[0,1]$ (notice that $0\leqslant\sin 2\phi\leqslant 1$ for $\phi\in[0,\pi/4]$) we parametrize the even and odd rates as $\Gamma_e=(1+\beta)\Gamma$, and $\Gamma_o=(1-\beta)\Gamma$, respectively. Thus, $\beta\neq 0$ accounts for processes where the even and odd channels are not coupled equally to the lead electrons or, equivalently, to processes where the orbital index is not conserved. Using the new notation, the mean field equations can be written in a compact way

$$\ln\left[\frac{(\tilde{\varepsilon}_0 + i\tilde{\Gamma}_e)}{D}\right] + \ln\left[\frac{(\tilde{\varepsilon}_0 + i\tilde{\Gamma}_o)}{D}\right] + \ln\left[\frac{\tilde{\varepsilon}_0^2+\tilde{\Gamma}_e^2}{\tilde{\varepsilon}_0^2+\tilde{\Gamma}_o^2}\right]^{\beta/2} = i\frac{\pi}{2} + \frac{\pi\varepsilon_0}{(\Gamma_e+\Gamma_o)} \tag{62}$$

or, equivalently,

$$[\tilde{\varepsilon}_0 + i\tilde{\Gamma}_e][\tilde{\varepsilon}_0 + i\tilde{\Gamma}_o]\left[\frac{\tilde{\varepsilon}_0^2+\tilde{\Gamma}_e^2}{\tilde{\varepsilon}_0^2+\tilde{\Gamma}_o^2}\right]^{\beta/2} = iD^2 e^{\pi\varepsilon_0/(\Gamma_e+\Gamma_o)}. \tag{63}$$

Its real and imaginary parts are

$$[\tilde{\varepsilon}_0^2 - \tilde{\Gamma}_e\tilde{\Gamma}_o]\left[\frac{\tilde{\varepsilon}_0^2+\tilde{\Gamma}_e^2}{\tilde{\varepsilon}_0^2+\tilde{\Gamma}_o^2}\right]^{\beta/2} = 0, \tag{64a}$$

$$\tilde{\varepsilon}_0(\tilde{\Gamma}_e + \tilde{\Gamma}_o)\left[\frac{\tilde{\varepsilon}_0^2+\tilde{\Gamma}_e^2}{\tilde{\varepsilon}_0^2+\tilde{\Gamma}_o^2}\right]^{\beta/2} = D^2 e^{\pi\varepsilon_0/(\Gamma_e+\Gamma_o)}. \tag{64b}$$

Equation (64a) has solution when $\tilde{\varepsilon}_0 = \pm\sqrt{\tilde{\Gamma}_e\tilde{\Gamma}_o}$. Notice that only the positive root satisfies Eq. (64b). By sustituting this result in Eq. (64b) we arrive after some algebra at

$$|\tilde{b}|^2 = \frac{D}{\sqrt{2}}\frac{1}{N\Gamma}\frac{(1-\beta)^{(\beta-1)/4}}{(1+\beta)^{(\beta+1)/4}} e^{\pi\varepsilon_0/2(\Gamma_e+\Gamma_o)}. \tag{65}$$

Using the previous result, we can define Kondo temperatures for each channel as[41]

$$T_K^e \equiv \sqrt{\tilde{\varepsilon}_0^2+\tilde{\Gamma}_e^2} = \frac{(1-\beta)^{(\beta-1)/4}}{(1+\beta)^{(\beta-1)/4}} D e^{\pi\varepsilon_0/2(\Gamma_e+\Gamma_o)},$$

$$T_K^o \equiv \sqrt{\tilde{\varepsilon}_0^2+\tilde{\Gamma}_o^2} = \frac{(1-\beta)^{(\beta+1)/4}}{(1+\beta)^{(\beta+1)/4}} D e^{\pi\varepsilon_0/2(\Gamma_e+\Gamma_o)}. \tag{66}$$

Using the above result we obtain the renormalized level position

$$\tilde{\varepsilon}_0 = \frac{D}{\sqrt{2}}\exp^{\pi\varepsilon_0/[2(\Gamma_e+\Gamma_o)]}\frac{(1-\beta)^{(\beta+1)/4}}{(1+\beta)^{(\beta-1)/4}}. \tag{67}$$

Equations (66) and (67), which are the main results of this section, give the Kondo temperatures and level position for arbitrary mixing $\beta$. Note that $\Gamma_e+\Gamma_o=2\Gamma$ does not depend on $\beta$ and therefore the Kondo temperature depends on orbital mixing only through the prefactor. $T_K^e$ changes very little as $\beta$ increases whereas $T_K^o$ decreases down to zero as $\beta\to 1$ (maximum mixing). Similarly, $\tilde{\varepsilon}_0$ goes from $T_K \equiv N\Gamma|\tilde{b}|^2(\beta=0)=\frac{D}{\sqrt{2}}\exp^{\pi\varepsilon_0/4\Gamma}$ to zero, in agreement with the Friedel sum rule. From the above results, we conclude that the odd orbital becomes decoupled at maximum mixing where we are left with SU(2) Kondo physics arising from spin fluctuations in the even orbital channel. This SU(4)→SU(2) transition as mixing increases is illustrated in Fig. 2 where we plot the

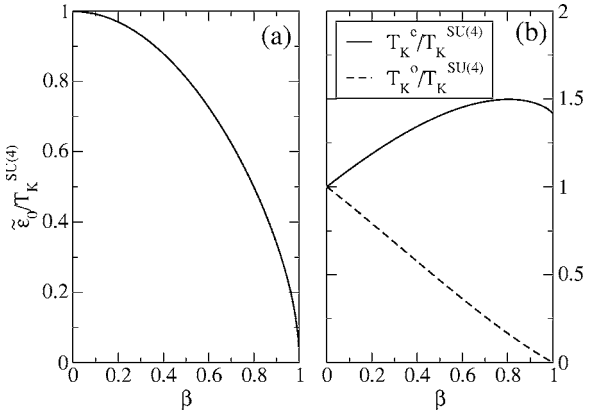


FIG. 13. Transition from SU(4) to SU(2) Kondo physics as obtainded from SBMFT: As the orbital mixing increases, the SU(4) Kondo effect reduces to an SU(2) spin Kondo effect. This is reflected in both the position of the Kondo resonance [Fig. 2(a)] as well as the reduction of the odd Kondo temperature down to zero [Fig. 2(b)], see main text.

SBMFT parameters as a function of $\beta$ (see Fig. 13).

Now we are in position to calculate transport properties. For this purpose it is now more convenient to write SBMFT equations in matrix form as (here we are back to the original basis)

$$|\tilde{b}^2| - \frac{1}{N}\int \frac{d\epsilon}{2\pi i}\mathrm{Tr}\hat{G}^<(\epsilon) = \frac{1}{N}, \tag{68a}$$

$$\lambda|\tilde{b}|^2 + \frac{1}{N}\int \frac{d\epsilon}{2\pi i}\mathrm{Tr}\{\hat{\Sigma}^r\hat{G}^<(\epsilon) + \hat{\Sigma}^<\hat{G}^a(\epsilon)\} = 0. \tag{68b}$$

The trace includes also the sum over spin indices. Here, $\hat{G}^<$ is the lesser matrix orbital Green function which is related to the advanced $\hat{G}^a$ and retarded $\hat{G}^r$ matrix Green functions through the expression

$$\hat{G}^< = \hat{G}^a\hat{\Sigma}^<\hat{G}^r, \tag{69}$$

where $\hat{\Sigma}^<$ is the lesser matrix self-energy. The explicit expressions for these matrices are

$$\hat{G}^a(\epsilon) = \frac{1}{(\epsilon - \tilde{\varepsilon}_0 - iT_K)^2 + \beta^2 T_K^2} \times \begin{pmatrix} \epsilon - \tilde{\varepsilon}_0 - iT_K & i\beta T_K \\ i\beta T_K & \epsilon - \tilde{\varepsilon}_0 - iT_K \end{pmatrix}. \tag{70}$$

($\hat{G}^r$ is obtained by direct complex conjugation of $\hat{G}^a$.) The lesser matrix self-energy reads

$$\hat{\Sigma}^< = -2i[f_L(\epsilon) + f_R(\epsilon)]\begin{pmatrix} T_K & \beta T_K \\ \beta T_K & T_K \end{pmatrix}. \tag{71}$$

In the same way the retarded matrix self-energy is

$$\hat{\Sigma}^r = -i\hat{\Gamma} = -i\begin{pmatrix} T_K & \beta T_K \\ \beta T_K & T_K \end{pmatrix}. \tag{72}$$

Inserting Eqs. (70) and (71) in Eq. (69) we obtain for the lesser orbital Green function

$$\hat{G}^< = \frac{-iT_K}{(\epsilon - \tilde{\varepsilon}_0)^4 + 2(1+\beta^2)T_K^2(\epsilon - \tilde{\varepsilon}_0)^2 + (\beta^2 - 1)^2 T_K^4}\begin{pmatrix} (\epsilon - \tilde{\varepsilon}_0)^2 + T_K(1-\beta^2) & \beta[(\epsilon - \tilde{\varepsilon}_0)^2 - T_K(1-\beta^2)] \\ \beta[(\epsilon - \tilde{\varepsilon}_0)^2 - T_K(1-\beta^2)] & (\epsilon - \tilde{\varepsilon}_0)^2 + T_K(1-\beta^2) \end{pmatrix}. \tag{73}$$

Using the explict expressions of the self-energies and the nonequilibrium Green functions we simplify Eq. (68b) as follows:

$$\lambda|\tilde{b}|^2 + \frac{1}{N}\int \frac{d\epsilon}{2\pi i}\mathrm{Tr}\hat{G}^<(\epsilon)(\epsilon - \tilde{\varepsilon}_0) = 0. \tag{74}$$

By solving in a self-consistent way Eqs. (68a) and (74) for each dc bias $V_{\mathrm{dc}}$, one gets the behavior of the two renormalized parameters at nonequilibrium conditions.[36]

The electrical current has in appearence the same form as the conventional Landauer-Büttiker current expression for noninteracting electrons

$$I = \frac{2e}{\hbar}\int \frac{d\epsilon}{2\pi}\mathcal{T}(\epsilon, V_{\mathrm{dc}})[f_L(\epsilon) - f_R(\epsilon)]. \tag{75}$$

Caution is needed in order to make a correct interpretation of Eq. (75), since it contains "many-body" effects via the renormalized parameters that have to be determined for each $V_{\mathrm{dc}}$ in a self-consistent way. As a result, $\mathcal{T}(\epsilon, V_{\mathrm{dc}})$ has a nontrivial behavior with voltage in contrast with the noninteracting case. The nonlinear conductance is calculated by direct derivation of Eq. (75) with respect to the bias voltage: $\mathcal{G} \equiv dI/dV_{\mathrm{dc}}$. In the limit of $V_{\mathrm{dc}} \to 0$ (at equilibrium) the linear conductance $\mathcal{G}_0$ is given by the well-known expression

$$\mathcal{G}_0 = \frac{2e^2}{h}\mathcal{T}(0), \tag{76}$$

where the transmission is

$$\mathcal{T}(\epsilon) = \mathrm{Tr}\{\hat{G}^a\hat{\Gamma}\hat{G}^r\hat{\Gamma}\}. \tag{77}$$

Finally, inserting Eqs. (70) and (72) in Eq. (77) one arrives at the explicit formula for the transmission

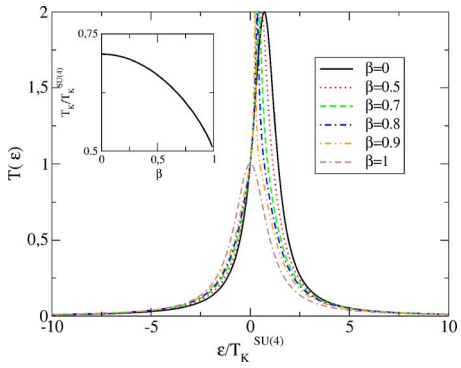


FIG. 14. (Color online) Equilibrium SBMFT result: Transmission, $\mathcal{T}(\epsilon)$ as a function of the frequency for several values of $\beta$. Left inset corresponds to the Kondo temperature vs $\beta$.

$$\mathcal{T}(\epsilon) = \frac{2T_K^2[(1+\beta^2)(\epsilon-\tilde{\varepsilon}_0)^2 + T_K^2(\beta^2-1)^2]}{(\epsilon-\tilde{\varepsilon}_0)^4 + 2(1+\beta^2)T_K^2(\epsilon-\tilde{\varepsilon}_0)^2 + (\beta^2-1)^2T_K^4}, \tag{78}$$

which is the main result of this part. Remarkably, the linear conductance $\mathcal{G}_0$ does not depend on $\beta$. In particular, for the SU(4) Kondo model ($\beta$=0), the transmission takes the simple form

$$\mathcal{T}(\epsilon) = \frac{2T_K^2}{[(\epsilon-\tilde{\varepsilon}_0)^2 + T_K^2]}. \tag{79}$$

In this case the resonance is pinned at $\epsilon=\tilde{\varepsilon}_0=T_K$ with a width given by $T_K$; this leads to $\mathcal{T}(0)=1$ and in consequence $\mathcal{G}_0 = 2e^2/h$. For $\beta$=1 [two-level SU(2) Kondo model] Eq. (78) reduces to

$$\mathcal{T}(\epsilon) = \frac{4T_K^2}{[(\epsilon-\tilde{\varepsilon}_0)^2 + 4T_K^2]}. \tag{80}$$

In this case the resonance occurs at $\epsilon=\tilde{\varepsilon}_0=0$ and again $\mathcal{T}(0)=1 \Rightarrow \mathcal{G}_0=2e^2/h$. As we pointed out, this fact makes both Kondo effects indistinguishable through linear conductance measurements.

All these features are clearly seen in Fig. 14 where the transmission for different amount of mixing, i.e., different $\beta$, is plotted. Thus, for $\beta$=0 the transmission peak is located at $T_K$ as expected whereas for $\beta$=1 this moves towards $\epsilon$=0. During the transition from the SU(4) to the two-level SU(2) Kondo model, the transmission gets narrower and develops a "cusp" signaling the competition between even and odd channels. This is clearly seen if we rewrite the transmission as follows:

$$\mathcal{T}(\epsilon) = \frac{(1+\beta)^2T_K^2}{[(\epsilon-\tilde{\varepsilon}_0)^2 + T_K^2(1+\beta)^2]} + \frac{(1-\beta)^2T_K^2}{[(\epsilon-\tilde{\varepsilon}_0)^2 + T_K^2(1-\beta)^2]}. \tag{81}$$

Note that both channels are resonant at the same energy $\tilde{\varepsilon}_0$ but have different widths ($\tilde{\Gamma}_e$ and $\tilde{\Gamma}_o$), which explains the "cusp" behavior. Here, we speculate that a finite splitting $\delta\varepsilon$ originated from charge fluctuations[42] (not included at the SBMFT level) would give rise to two split resonances for $\beta \neq 0$, namely, $\tilde{\varepsilon}_0 \rightarrow \tilde{\varepsilon}_0^{\pm} = \delta\varepsilon \pm \sqrt{\tilde{\Gamma}_e\tilde{\Gamma}_o}$. This is confirmed in the next section where we present results obtained from a full NCA calculation including fluctuations. Eventually, for $\beta$ =1 the competition cannot occur and the transmission does not show the cusp.

### B. Noncrossing approximation method

The SBMFT suffers from two drawbacks: (1) it leads always to local Fermi liquid behavior and (2) The SBMFT has a phase transition (originating from the breakdown of the local gauge symmetry of the problem) that separates the low temperature state from the high temperature local moment regime. This later problem may be corrected by including 1/N corrections around the mean-field solution. The noncrossing approximation (NCA)[43–45] is the lowest order self-consistent, fully conserving and $\Phi$ derivable theory in the Baym sense[46] which includes such corrections. Without entering into much detail of the theory, we just mention that the boson fields in Eq. (54), which were treated as averages in the previous subsection $[b(t)/\sqrt{N} \rightarrow \langle b\rangle/\sqrt{N} \equiv \tilde{b}]$, are treated now as fluctuating quantum objects. In particular, one has to derive self-consistent equations-of-motion for the time-ordered double-time Green's function (subindexes are omitted here)

$$iG(t,t') \equiv \langle T_c f(t) f^{\dagger}(t')\rangle,$$

$$iB(t,t') \equiv \langle T_c b(t) b^{\dagger}(t')\rangle \tag{82}$$

or in terms of their analytic pieces

$$iG(t,t') = G^{>}(t,t')\theta(t-t') - G^{<}(t,t')\theta(t'-t),$$

$$iB(t,t') = B^{>}(t,t')\theta(t-t') + B^{<}(t,t')\theta(t'-t). \tag{83}$$

A rigorous and well established way to derive these equations-of-motion was first introduced by Kadanoff and Baym,[47] and has been related to other nonequilibrium methods (like the Keldysh method) by Langreth, see Ref. 40 for a review. Here, we just show numerical results of the NCA equations for our problem and refer the interested reader to Refs. 38 and 43–45 for details.

In particular, the density of states is given by

$$\rho(\varepsilon) = -\frac{1}{\pi}\sum_{\nu=e,o,\sigma} \mathrm{Im}[A^r_{\nu\sigma}(\varepsilon)], \tag{84}$$

where $A^r_{\nu\sigma}(\varepsilon)$ is the Fourier transform of the retarded Green function

$$A^r_{\nu\sigma}(t) = G^r_{\nu,\sigma}(t)B^{<}(-t) - G^{<}_{\nu\sigma}(t)B^a(-t). \tag{85}$$

The density of states for different values of $\beta$, and different temperatures, is plotted in Fig. 15. Interestingly, the cusp behavior of Fig. 14 in the previous subsection now becomes a splitting for the even and odd channels. This is illustrated in the inset where the curve corresponding to $\beta$=0.5 is plotted together with the individual even and odd channel contributions. As we anticipated, the presence of charge fluctuations yields the splitting of $\varepsilon_0$ s due to the different

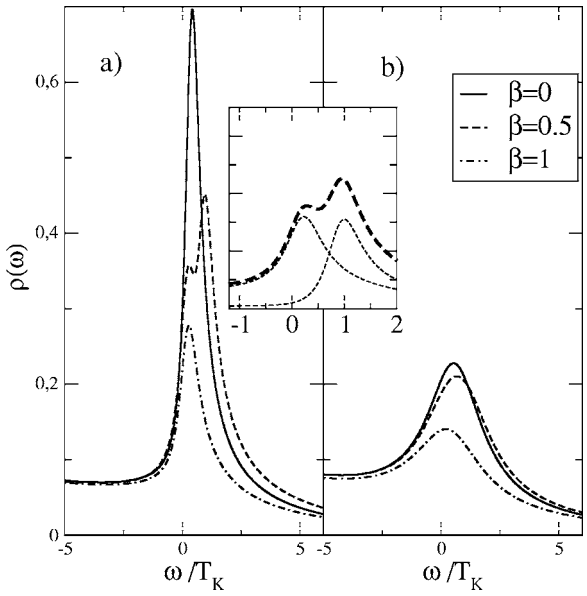


FIG. 15. NCA results: Density of states around $\varepsilon=0$ for $T=0.25T_K$ (left) and $T=T_K$ (right) and different values of $\beta$. The inset shows a close-up for the $\beta=0.5$ curve (thick dashed) together with the individual even and odd channel contributions (thin dashed).

renormalization arising from different couplings for the even and odd channels ($\Gamma_{e(o)}$) [see Eqs. (38) and (39)].

## V. CONCLUSION

We have considered the single-electron transistor (SET) device with the CNT QD or VQD as the central island in the Kondo regime. We studied the case where the CNT QD or VQD has a high symmetry so that the orbital quantum numbers are conserved through the system. We investigated in detail how different Kondo physics, the SU(4) Kondo effect or the two-level SU(2) Kondo effect, emerges depending on the extent to which the symmetry is broken in realistic situations. We used four different theoretical approaches, the scaling theory, the NRG method, the SBMFT, and the NCA method to address both the linear and nonlinear conductance for different values of external magnetic field. Our results show that there is no way to distinguish experimentally by means of the linear conductance (low-energy property) alone. The SU(4) Kondo physics, which arises with higher symmetry, can be observed exclusively only by the nonlinear conductance (higher-energy property) in the presence of finite mangetic field, as in the recent experiment.[9,48] The symmetry breaking (either the orbital anisotropy $1-\Gamma_2/\Gamma_1$ or the orbital mixing $\Gamma_X$) drives the system from the SU(4) Kondo fixed point to the SU(2) Kondo fixed point. At finite yet sufficiently small symmetry breaking, the SU(4) Kondo phyiscs governs the transport in the system at relatively high energies (order of the Kondo temperature) while the two-level SU(2) Kondo effect takes it over at extremely low energies. This gives another reason why the indications of the SU(4) Kondo physics should be investigated by means of the nonlinear conductance in the presence of external magnetic field.

## ACKNOWLEDGMENTS

This work was supported by the MEC of Spain (Grants Nos. FIS2005-02796, MAT2005-07369-C03-03, and the Ramon y Cajal Program), by CSIC (Proyecto Intramural Especial I3), the SRC/ERC program of MOST/KOSEF (Grant No. R11-2000-071), the Korea Research Foundation (Grant No. KRF-2005-070-C00055), the SK Fund, and the KIAS.

## APPENDIX: NUMERICAL RENORMALIZATION GROUP

The Hamiltonian (3) allows both the charge fluctuations and spin fluctuations. The charge fluctuations (accompanied by the particle-hole excitations) occur at high energies while the spin fluctuations prevail at low energies. Therefore in order to understand the low-energy properties of the system, it is useful to take a renormalization group (RG) approach and to obtain an effective Hamiltonian allowing only the spin fluctuations. One can take three-state perturbative RG procedures (scaling theory): one first renormalizes the Anderson-type Hamiltonian (3) until the charge fluctuations are completely suppressed[17,18] (see also Ref. 27), perform the Schrieffer-Wolf (SW) transformation[49] to obtain a Kondo-type Hamiltonian where the spin fluctuations are described by the spin operators, and renormalize further the resulting Kondo-type Hamiltonian.[16] The RG equations of the coupllng constants in the Hamiltonian allow us to identify the physically interesting fixed points and associated scaling properties.

We follow the standard procedures to implement the NRG calculations.[19–21] We evaluate the various physical quantities from the recursion relation ($N \geqslant 0$)

$$\tilde{H}_{N+1} = \sqrt{\Lambda}\tilde{H}_N + \xi_{N+1}\sum_{\mu\sigma}(f^{\dagger}_{\mu,N,\sigma}f_{\mu,N+1,\sigma} + \text{H.c.}), \quad \text{(A1)}$$

with the initial Hamiltonian given by

$$\tilde{H}_0 = \frac{1}{\sqrt{\Lambda}}\left[\tilde{H}_D + \sum_{\mu m}\sum_{\sigma}\tilde{V}_{\mu,m}(f^{\dagger}_{\mu,0,\sigma}d_{m\sigma} + \text{H.c.})\right]. \quad \text{(A2)}$$

Here the fermion operators $f_{\mu,N,\sigma}$ have been introduced as a result of the logarithmic discretization and the accompanying canonical transformation, $\Lambda$ is the logarithmic discretization parameter (we choose $\Lambda=2$),

$$\xi_N \equiv \frac{1-\Lambda^{-N}}{\sqrt{[1-\Lambda^{-(2N-1)}][1-\Lambda^{-(2N+1)}]}}, \quad \text{(A3)}$$

and

$$\tilde{H}_D \equiv \zeta\frac{H_D}{D} \quad \text{(A4)}$$

with $\zeta=2/1+1/\Lambda$. The coupling constants $\tilde{V}_{\mu,m}$ have been defined by

$$\tilde{V}_{\mu,m} \equiv \sqrt{\frac{2\rho_0|V_{\mu,m}|^2}{\pi D}}, \quad \text{(A5)}$$

where $\rho_0$ is the density of states of the leads at the Fermi energy. The Hamiltonians $\tilde{H}_N$ in Eq. (A1) have been rescaled

for numerical accuracy. The original Hamiltonian is recovered by

$$\frac{H}{D} = \lim_{N\to\infty} \frac{\tilde{H}_N}{\mathcal{S}_N}, \tag{A6}$$

with $\mathcal{S}_N \equiv \zeta \Lambda^{(N-1)/2}$. At each iteration of the NRG procedures, we calculate the local spectral density,[50] which determines the transport properties through the dot

$$A_{mm'}(\omega) = A^{>}_{mm'}(\omega) - A^{<}_{mm'}(\omega) \tag{A7}$$

with

$$A^{>}_{mm';\sigma}(E) = +\sum_{\alpha} \langle 0|d_{m\sigma}|\alpha\rangle\langle\alpha|d^{\dagger}_{m'\sigma}|0\rangle \delta(E - E_{\alpha} + E_0), \tag{A8a}$$

$$A^{<}_{mm';\sigma}(E) = -\sum_{\alpha} \langle 0|d^{\dagger}_{m'\sigma}|\alpha\rangle\langle\alpha|d_{m\sigma}|0\rangle \delta(E + E_{\alpha} - E_0), \tag{A8b}$$

where $|0\rangle$ ($|\alpha\rangle$) is the many-body ground (excited) state of the system and $E_0$ ($E_{\alpha}$) the corresponding energy.

*Electronic address: choims@korea.ac.kr


[1] D. Goldhaber-Gordon, H. Shtrikman, D. Mahalu, D. Abusch-Magder, U. Meirav, and M. A. Kastner, Nature (London) **391**, 156 (1998); D. Goldhaber-Gordon, J. Göres, M. A. Kastner, Hadas Shtrikman, D. Mahalu, and U. Meirav, Phys. Rev. Lett. **81**, 5225 (1998).

[2] S. M. Cronenwett, T. H. Oosterkamp, and L. P. Kouwenhoven, Science **281**, 540 (1998).

[3] J. Schmid, J. Weis, K. Eberl, and K. v. Klitzing, Physica B **256-258**, 182 (1998).

[4] W. G. van der Wiel, S. De Franceschi, T. Fujisawa, J. M. Elzerman, S. Tarucha, and L. P. Kouwenhoven, Science **289**, 2105 (2000).

[5] S. Sasaki, S. De Franceschi, J. M. Elzerman, W. G. van der Wiel, M. Eto, S. Tarucha, and L. P. Kouwenhoven, Nature (London) **405**, 764 (2002).

[6] Jiwoong Park, Abhay N. Pasupathy, Jonas I. Goldsmith, Connie Chang, Yuval Yaish, Jason R. Petta, Marie Rinkoski, James P. Sethna, Hector D. Abrua, Paul L. McEuen, and Daniel C. Ralph, Nature (London) **417**, 722 (2002); Wenjie Liang, Matthew P. Shores, Marc Bockrath, Jeffrey R. Long, and Hongkun Park, *ibid.* **417**, 725 (2002).

[7] Abhay Pasupathy, Radoslaw Bialczak, Jan Martinek, Jacob Grose, Luke Doney, Paul McEuen, and Daniel Ralph, Science **306**, 86 (2004).

[8] M. R. Buitelaar, T. Nussbaumer, and C. Schönenberger, Phys. Rev. Lett. **89**, 256801 (2002).

[9] P. Jarillo-Herrero, J. Kong, H. S. J. van der Zant, C. Dekker, L. P. Kouwenhoven, and S. De Franceschi, Nature (London) **434**, 484 (2005).

[10] M.-S. Choi, R. López, and R. Aguado, Phys. Rev. Lett. **95**, 067204 (2005).

[11] Rui Sakano and Norio Kawakami, Phys. Rev. B **73**, 155332 (2006).

[12] E. D. Minot, Y. Yaish, V. Sazonova, and P. L. McEuen, Nature (London) **428**, 536 (2004).

[13] J. Cao, Q. Wang, M. Rolandi, and H. Dai, Phys. Rev. Lett. **93**, 216803 (2004).

[14] S. Sasaki, S. Amaha, N. Asakawa, M. Eto, and S. Tarucha, Phys. Rev. Lett. **93**, 017205 (2004).

[15] Here, we focus on quarter filling. For half filling, an interesting quantum phase transition involving SU(4) symmetry has been discussed in M. R. Galpin, D. E. Logan, and H. R. Krishnamurthy, Phys. Rev. Lett. **94**, 186406 (2005).

[16] P. W. Anderson, J. Phys. C **3**, 2436 (1970).

[17] F. D. M. Haldane, Phys. Rev. Lett. **40**, 416 (1978), see also Ref. 18.

[18] F. D. M. Haldane, Phys. Rev. Lett. **40**, 911 (1978).

[19] K. G. Wilson, Rev. Mod. Phys. **47**, 773 (1975).

[20] H. R. Krishnamurthy, J. W. Wilkins, and K. G. Wilson, Phys. Rev. B **21**, 1003 (1980).

[21] T. A. Costi, A. C. Hewson, and V. Zlatic, J. Phys.: Condens. Matter **6**, 2519 (1994).

[22] W. Hofstetter, Phys. Rev. Lett. **85**, 1508 (2000).

[23] Y. Meir and N. S. Wingreen, Phys. Rev. Lett. **68**, 2512 (1992).

[24] D. C. Langreth, Phys. Rev. **150**, 516 (1966).

[25] Y. Kuramoto, Eur. Phys. J. B **5**, 457 (1998).

[26] M. Eto, J. Phys. Soc. Jpn. **74**, 95 (2004), special issue on "Kondo Effect—40 Years after the Discovery."

[27] D. Boese, W. Hofstetter, and H. Schoeller, Phys. Rev. B **66**, 125315 (2002).

[28] Y. Meir, N. S. Wingreen, and P. A. Lee, Phys. Rev. Lett. **70**, 2601 (1993).

[29] N. S. Wingreen and Y. Meir, Phys. Rev. B **49**, 11040 (1994).

[30] W. Izumida, O. Sasakai, and Y. Shimizu, J. Phys. Soc. Jpn. **66**, 717 (1997).

[31] T. Aono and M. Eto, Phys. Rev. B **63**, 125327 (2001).

[32] B. Dong and X. L. Lei, J. Phys.: Condens. Matter **14**, 4963 (2002).

[33] R. López and D. Sánchez, Phys. Rev. Lett. **90**, 116602 (2003).

[34] Y. Avishai, A. Golub, and A. D. Zaikin, Phys. Rev. B **67**, 041301(R) (2003).

[35] A. Georges and Y. Meir, Phys. Rev. Lett. **82**, 3508 (1999).

[36] R. Aguado and D. C. Langreth, Phys. Rev. Lett. **85**, 1946 (2000).

[37] R. Lopez, R. Aguado, and G. Platero, Phys. Rev. Lett. **89**, 136802 (2002); Phys. Rev. B **69**, 235305 (2004).

[38] R. Aguado and D. C. Langreth, Phys. Rev. B **67**, 245307 (2003).

[39] P. Simon, R. Lopez, and Y. Oreg, Phys. Rev. Lett. **94**, 086602 (2005).

[40] D. C. Langreth, in *Linear and Nonlinear Electron Transport in Solids*, Nato ASI, Series B, Vol. 17, edited by J. T. Devreese and V. E. Van Doren (Plenum, New York, 1976).

[41] A. C. Hewson, *The Kondo Problem to Heavy Fermions* (Cambridge University Press, Cambridge, UK, 1993).

[42] M.-S. Choi, R. López, and D. Sánchez, Phys. Rev. Lett. **92**, 056601 (2004).

[43] David C. Langreth and Peter Nordlander, Phys. Rev. B **43**, 2541 (1991).
[44] Ned S. Wingreen and Yigal Meir, Phys. Rev. B **49**, 11040 (1994).
[45] Matthias H. Hettler, Johann Kroha, and Selman Hershfield, Phys. Rev. Lett. **73**, 1967 (1994); Phys. Rev. B **58**, 5649 (1998).
[46] G. Baym and L. P. Kadanoff, Phys. Rev. **124**, 287 (1961); G. Baym, *ibid.* **127**, 1391 (1962).
[47] L. P. Kadanoff and G. Baym, *Quantum Statistical Mechanics* (Benjamin, New York, 1962).
[48] P. Jarillo-Herrero, J. Kong, H. S. J. van der Zant, C. Dekker, L. P. Kouwenhoven, and S. De Franceschi, Phys. Rev. Lett. **94**, 156802 (2005).
[49] J. R. Schrieffer and P. A. Wolff, Phys. Rev. **149**, 491 (1966).
[50] R. Bulla, T. A. Costi, and D. Vollhardt, Phys. Rev. B **64**, 045103 (2001).